Low Temperature Plasma
Technology Laboratory

Instability Driven Radial Transport in a Helicon Plasma

Max Light, Francis F. Chen, and Pat Colestock

LTP-101 January, 2001

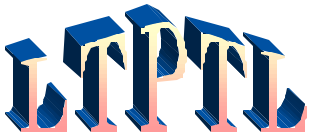

Electrical Engineering Department
Los Angeles, California 90095-1594

Anomalous Particle Transport in a Helicon Plasma

Max Light

Los Alamos National Laboratory, Los Alamos, New Mexico 87545

Francis F. Chen

Electrical Engineering Department, University of California, Los Angeles, California 90095-1594

P. L. Colestock

Los Alamos National Laboratory, Los Alamos, New Mexico 87545

(May 29, 2001)

Abstract

Known for their ability to produce high densities at low power, helicon discharges have found many practical uses. However, with light gases it has been found that the plasma density saturates, then falls, as the magnetic field is increased. This can be explained by the onset of a drift-type instability, whose threshold agrees well with linear theory. Measurements of radial and axial particle fluxes show that the enhanced losses occur via a new mechanism: The fluctuation-induced radial transport stops short of the boundary and serves only to move plasma into flux tubes of larger cross section, where it is lost by axial flow.

52.25.Fi, 52.25.Gj, 52.35.-g, 52.50.Dg

Typeset using REVTEX

Helicons are cylindrically bounded whistler waves lying on the fast R-wave dispersion branch of electromagnetic plasma waves [1–4]. Radio-frequency (rf) plasma sources based on helicons are noted for their unusually high ionization efficiency. These sources are used in plasma processing of semiconductors, ionospheric plasma research, ion lasers, general plasma physics experiments, and plasma thruster research [5–10]. Sakawa et al [11] have reported that the plasma density n in this discharge does not monotonically increase with magnetic field strength in light gases. This has also been observed in several other helicon experiments [12–15]. Furthermore, the possibility of ion mass effects in these discharges has been borne out by the work of Scime et. al [6]. Efforts to increase the maximum attainable plasma density in these sources are driven by their applicability to space propulsion. Arguably the most important characteristic of magnetized plasma sources is the scaling of equilibrium density with magnetic field strength, $n_0(B_0)$, and understanding the physics behind this trend is critical.

Investigation of the $n_0(B_0)$ scaling was performed on the apparatus shown in Fig. 1, with magnetic field strength $\leq 1.5\ kG$ and $2\ kW$ of $13.56\ MHz$ power into a right-helical [16] antenna. Gas fill pressure was kept constant at $8\ mTorr$, and neutral depletion effects were determined to be negligible. Characterization of fluctuations was done by measuring the magnitude and phase of density and floating potential fluctuations $(\tilde{n}, \tilde{\phi})$ with a triple-probe technique employed in magnetic fusion [17,18]. $\tilde{E}$ was determined from the relation $\tilde{E} = -ik_\theta\tilde{\phi}$; where k_θ is the azimuthal wavenumber calculated from the phase difference between the two probe tips measuring $\tilde{\phi}$. Density fluctuations were measured by biasing the third tip well into the ion saturation regime. Radial profiles of the azimuthal wavenumber at various B_0 revealed a discrete azimuthal mode structure. All measurements were taken $30\ cm$ downstream of the antenna mid-plane, unless specified otherwise.

Measurements of $n_0(B_0)$ are given in Fig 2b for all gases used in this experiment. This figure also shows a spectrogram of the density fluctuations $\tilde{n}(B_0)$ in neon. Note that the saturation in plasma density and onset of strong, low-frequency fluctuations in $\tilde{n}$ occur at the same magnetic field, which will be referred to as B_{crit}. This correlation was seen in

all gases used in the experiment, and B_{crit} increased with increasing ion mass. Heavier gases (neon, argon) showed a saturation, while the light gases (hydrogen, helium) suffered a decrease in plasma density beyond B_{crit}. Fig. 2c shows the magnitude of the dominant frequency component of $\tilde{n}$ fluctuations in helium, illustrating the onset of strong low-frequency fluctuations that continue to grow past B_{crit}.

The instability threshold can be predicted from a two fluid model employing the usual linear perturbation technique [19] to describe the fluctuating quantities $\tilde{n}$ and $\tilde{\phi}$ in a slab geometry. Collision rates were dominated by neutrals. Ions were assumed to be at room temperature, thus eliminating magnetic viscosity effects; electron inertia was neglected; fluctuations were assumed to be electrostatic ($\beta \ll 1$ for this experiment) and were Fourier-analyzed in the θ (y) and z directions; wave-particle resonance effects were neglected; and the density $n_0(x)$ and space potential $V_s(x)$ profiles were allowed to vary. Perturbations had the form $exp[i(m\theta + k_z z - \omega t)]$, and were assumed to be absolute, with k_z real and $\omega = \omega_R + i\gamma_I$ complex. The detected fluctuations had ω small enough to justify the ordering

$$\omega, \omega_{EB}(x), \omega_*(x) \ll \Omega_c \tag{1}$$

where the $E_{0x} \times B_{0z}$ drift, electron diamagnetic drift, and ion cyclotron frequencies are defined respectively by

$$\omega_{EB}(x) = k_y v_E(x) = k_y \frac{V_s'(x)}{B_0}$$

$$\omega_*(x) = k_y \frac{KT_e}{eB_0} \frac{n_0'(x)}{n_0(x)}; \quad \Omega_c = \frac{eB_0}{M_i} \quad . \tag{2}$$

In the above equations, k_y is the azimuthal wavenumber; x corresponds to the radial coordinate in a slab geometry; and $'$ denotes $\partial/\partial x$.

Coupling the linearized equations of motion and continuity for each species in a singly ionized plasma via the plasma approximation $n_i = n_e$ results in a quartic dispersion relation

$$0 = \frac{\hat{\omega}}{C_s^2} \left(\frac{-\omega_* \nu_e + i k_z^2 v_{th}^2}{\hat{\omega} \nu_e + i k_z^2 v_{th}^2} \right) + \frac{(k_x^2 + k_y^2)(\hat{\omega} + i\nu_i)}{\Omega_c (\Omega_c + v_E')}$$

$$-\frac{ik_x n_0'/n_0(\hat{\omega}+i\nu_i)}{\Omega_c(\Omega_c+v_E')}+\frac{k_y n_0'/n_0}{\Omega_c+v_E'}-\frac{k_z^2}{\hat{\omega}+i\nu_e}$$

$$+\frac{i2k_xk_yv_E'(\hat{\omega}+i\nu_i)^2}{\Omega_c^2(\Omega_c+v_E')^2}-\frac{2k_y^2v_E'(\hat{\omega}+i\nu_i)}{\Omega_c(\Omega_c+v_E')^2} \quad , \tag{3}$$

where ν_j is the collision rate for each species, v_{th} the electron thermal velocity, C_s the ion sound speed, and $\hat{\omega}=\omega-\omega_{EB}$ the doppler shifted eigenfrequency. The problem was re-cast in cylindrical geometry, and radial eigenfunctions of $\tilde{n}$ and $\tilde{\phi}$ were found as well. Equation 3 yields the local frequency and growth rate for a given set of measured equilibrium profiles $n_0(x), V_s(x)$, and parameters B_0, T_e, and M_i. The perpendicular flux driven by the fluctuations, $\Gamma_\perp =< \tilde{n}\tilde{v} >$, was computed using $\tilde{n}$ from the ion continuity equation along with $\tilde{v}$ from the ion equation of motion, giving a function that depended on the magnitude of $\tilde{\phi}$ and $\theta_{n\phi}$, the phase angle between $\tilde{n}$ and $\tilde{\phi}$.

Fig. 2c shows the variation of the predicted growth rate γ with B_0, along with the measured magnitude of the low frequency fluctuations in $\tilde{\phi}$ and $\tilde{n}$ in helium. Measured fluctuation frequencies were consistent with predicted values. The maximum predicted growth rate is in excellent agreement with the measured maximum in $|\tilde{\phi}|$ and onset of strong fluctuations in $|\tilde{n}|$. The model predicted instability onset for all gases used in the experiment, as shown in Fig. 3. Note that the predicted growth rate in Fig. 2c decreases after reaching a maximum, while $\tilde{n}/n_0$ continues to grow. This is due to the linear nature of the model, which correctly predicts behavior up to just beyond the onset, but not in the turbulent saturated regime.

The triple probe used in this experiment allowed direct measurement of the radial flux $\Gamma_\perp$ driven by the instability at discreet radii [18]. This is compared in Fig. 2d to the predicted radial flux calculated from the measurement of $|\tilde{\phi}|$ and $\theta_{n\phi}$. Note that the instability onset(Fig. 2c), saturation (before decrease) in $n_0(B_0)$ (Fig. 2b), predicted maximum growth rate(Fig. 2c), and maximum in $\Gamma_\perp$ (Fig. 2d) are all correlated to the same $B_{crit} \approx 760G$ for helium.

The behavior of $\Gamma_\perp$ with radius in helium, given in Fig. 4, shows that $\Gamma_\perp(r)$ is restricted

to the interior of the plasma column. This localization was observed over the entire range of B_0 in Fig. 2d where $\Gamma_\perp(r)$ was significant.

The measurement of $\tilde{n}(B_0)$ in Fig. 2c shows that the discharge has entered a strongly turbulent regime above B_{crit}. Direct correlation of $n_0(B_0)$ with instability characteristics becomes extremely difficult. The fluctuation-driven radial flux decreases instead of remaining constant and is localized in radius. This appears to be inconsistent with the density decrease at the highest magnetic fields, unless their is another loss mechanism. Axial loss was thus investigated by measuring radial profiles of the ion axial flow velocity in terms of the mach number M [20], where $v_{||i} = MC_s$, at the antenna mid-plane. These are shown in Fig. 5 and indicate a greatly enhanced axial loss above B_{crit}.

An explanation can be formulated by considering both the axial and radial losses. Consider dividing the plasma column in to two regions, a central tube of radius $2cm$ and an outer shell extending from $r = 2cm$ [where $\Gamma_\perp(B_0)$ was measured] to the outer boundary. Before the instability onset, axial losses from the outer shell dominate. In the region of B_0 where the instability is growing and $\Gamma_\perp$ is strong, axial losses in the central region are starting to become significant, while radial losses are greatly enhanced, thus transporting particles to the outer shell region. These particles, along with the background ones, are then lost axially over a larger cross-sectional area than that of the central region and hence generate a greater loss rate. At the highest B_0, Fig. 5 shows that axial losses are much larger than at lower fields and that they occur mostly in the outer shell.

We have found that the saturation of $n_0(B_0)$ correlates with the onset of a low-frequency instability whose characteristics agree with theory in the linear regime. At fields well beyond the threshold, $\tilde{n}$ continues to increase and n_0 to decrease with B_0, but the $< \tilde{n}\tilde{\phi} >$ correlation shows that the radial flux maximizes at $r \approx 2cm$, falling to ≈ 0 at the edge, as if there were an internal transport barrier. The loss is then dominated by axial loss to the endplates at the acoustic velocity, the radial transport serving only to move plasma into flux tubes of larger cross-section. At the highest magnetic field of $1500G$, the radial flux appears to be small everywhere, but we suspect that the $< \tilde{n}\tilde{\phi} >$ correlation technique fails in this highly

turbulent regime. Thus, the n_0 vs. B_0 behavior of helicon discharges is in good agreement with linear instability theory in regions in which that theory is applicable.

The authors wish to thank G. Tynan for useful discussions.

REFERENCES

[1] F. F. Chen, Plasma Phys. and Controlled Fusion, **3**, 339 (1991).

[2] M. A. Liebermann and A. J. Lichtenberg, *Principles of Plasma Discharges and Materials Processing* (Wiley, New York, 1994).

[3] R. W. Boswell and F. F. Chen, I.E.E.E. Trans. on Plasma Sci., **25**, 1229 (1997).

[4] F. F. Chen and D. Arnush, Phys. Plasmas, **4**, 3411 (1997).

[5] M. A. Liebermann and R. A. Gottscho in G. Hass, editor, *Physics of Thin Films* (Academic, New York, 1994).

[6] E. E. Scime, P. A. Keiter, M. W. Zintl, M. M. Balkey, J. L. Kline, and M. Koepke, Plasma Sources Sci. Technol., **7**, 186 (1998).

[7] P. Zhu and R. W. Boswell, Phys. Rev. Lett., **63**, 2805 (1989).

[8] B. N. Breizman and A. V. Arefiev, Phys. Rev. Lett., **84**, 3863 (2000).

[9] F. F. Chen and D. D. Blackwell, Phys. Rev. Lett., **82**, 2677 (2000).

[10] F. R. Chang Diaz, J. P. Squire, R. D. Bengston, B. N. Breizmann, F. W. Baity, and M. D. Carter, in *Proceedings of the 36th AIAA/ASME/ASEE Joint Propulsion Conference*, No. 2000-3756 (2000).

[11] Y. Sakawa, T. Takino, and T. Shoji, Phys. Plasmas, **6**, 4759 (1999).

[12] A.J. Perry and R.W. Boswell, J. Vac. Sci. Technol. B, **9**, 310 (1991).

[13] J.H. Kim and H.Y. Chang, Phys. Plasmas, **3**, 1462 (1996).

[14] P.A. Keiter, E.E. Scime, and M.M. Balkey, Phys. Plasmas, **4**, 2741 (1997).

[15] D.A. Schneider, D.D. Borg, and I.V. Kamenski, Phys. Plasmas, **6**, 703 (1999).

[16] M. Light and F.F. Chen, Phys. Plasmas, **2**, 1084 (1995).

[17] J.M. Beall, Y.C. Kim, and E.J. Powers, J. Appl. Phys., **53**, 3933 (1982).

[18] E.J. Powers, Nucl. Fusion, **14**, 749 (1974).

[19] N. A. Krall and A. W. Trivelpiece, *Principles of Plasma Physics* (San Francisco Press, San Francisco, 1986).

[20] P.C. Stangeby, Phys. Fluids, **27**, 2699 (1984).

FIGURES

FIG. 1. Experimental apparatus. The magnetic field was uniform to within a few percent over the length specified by the dashed arrow. The chamber diameter was 15.2 cm, and the overall length 1.97 m.

FIG. 2. Parameters versus B_0. (a) Frequency spectrum in neon measured with a langmuir probe biased to ion saturation. $L = -24.5\ dBm$ and $H = -10.1\ dBm$. (b) Electron density ($10^{13}/cm^3$) for all gases used in the experiment. (c) Measured fluctuation amplitudes, in helium, of density ($\tilde{n}/n_0$, connected points), potential ($\tilde{\phi}/T_e$, open points connected by a line), and calculated instability growth rate (γ, line). Parameters used in model: $k_x = 52/m, k_y = 16.7/m, k_z = 0.5/m, \nu_e = 10^8/sec, \nu_i = 10^3/sec$. (d) Measured (connected points) and calculated (line) radial flux driven by instability ($10^{21} m^{-2} s^{-1}$) at $r = 2cm$.

FIG. 3. Predicted and measured B_{crit} versus ion mass number A.

FIG. 4. Measured $\Gamma_\perp$ versus radius at different B_0 in helium.

FIG. 5. Measured ion mach number at antenna mid-plane versus radius at different B_0 in helium.

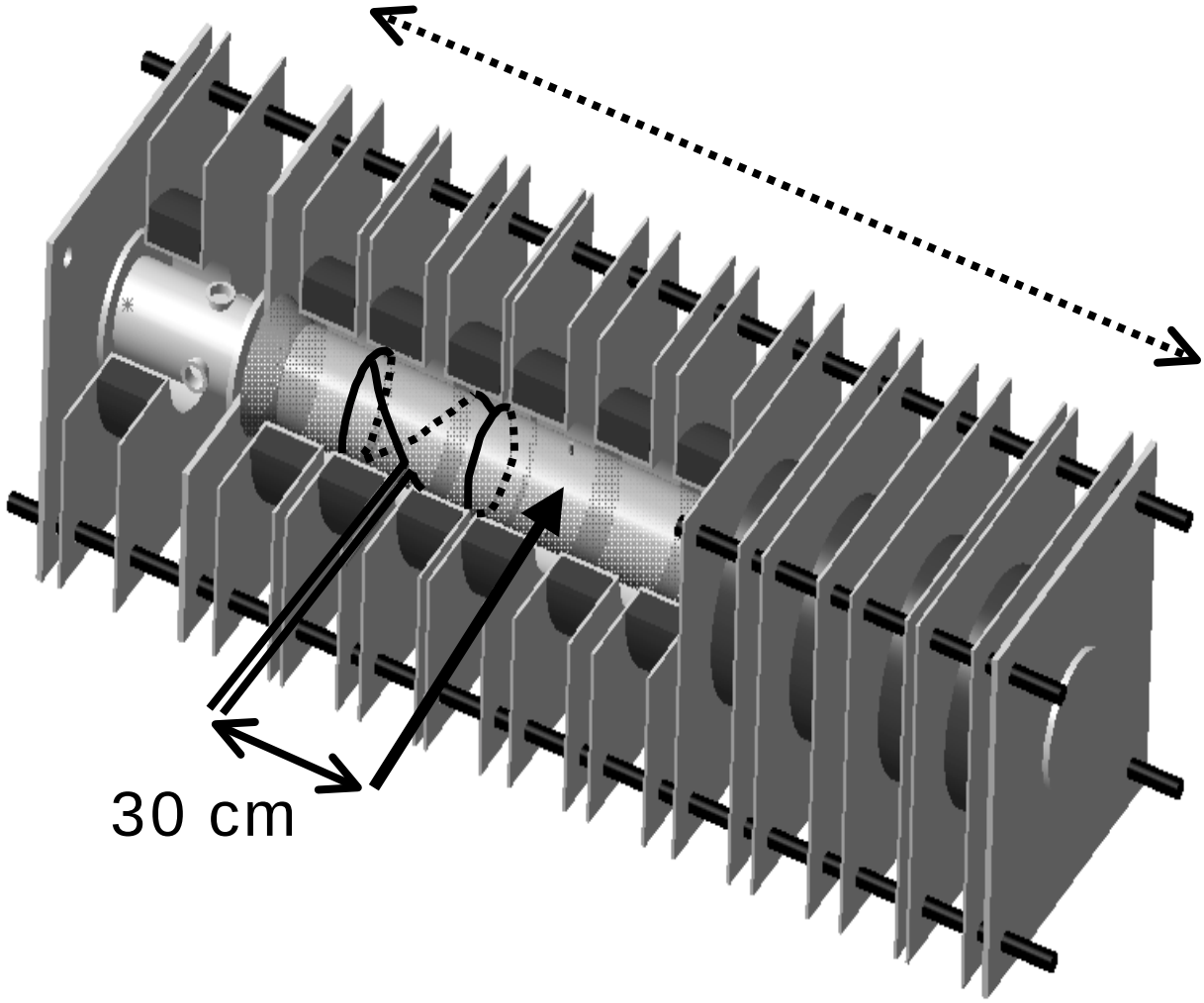
30 cm

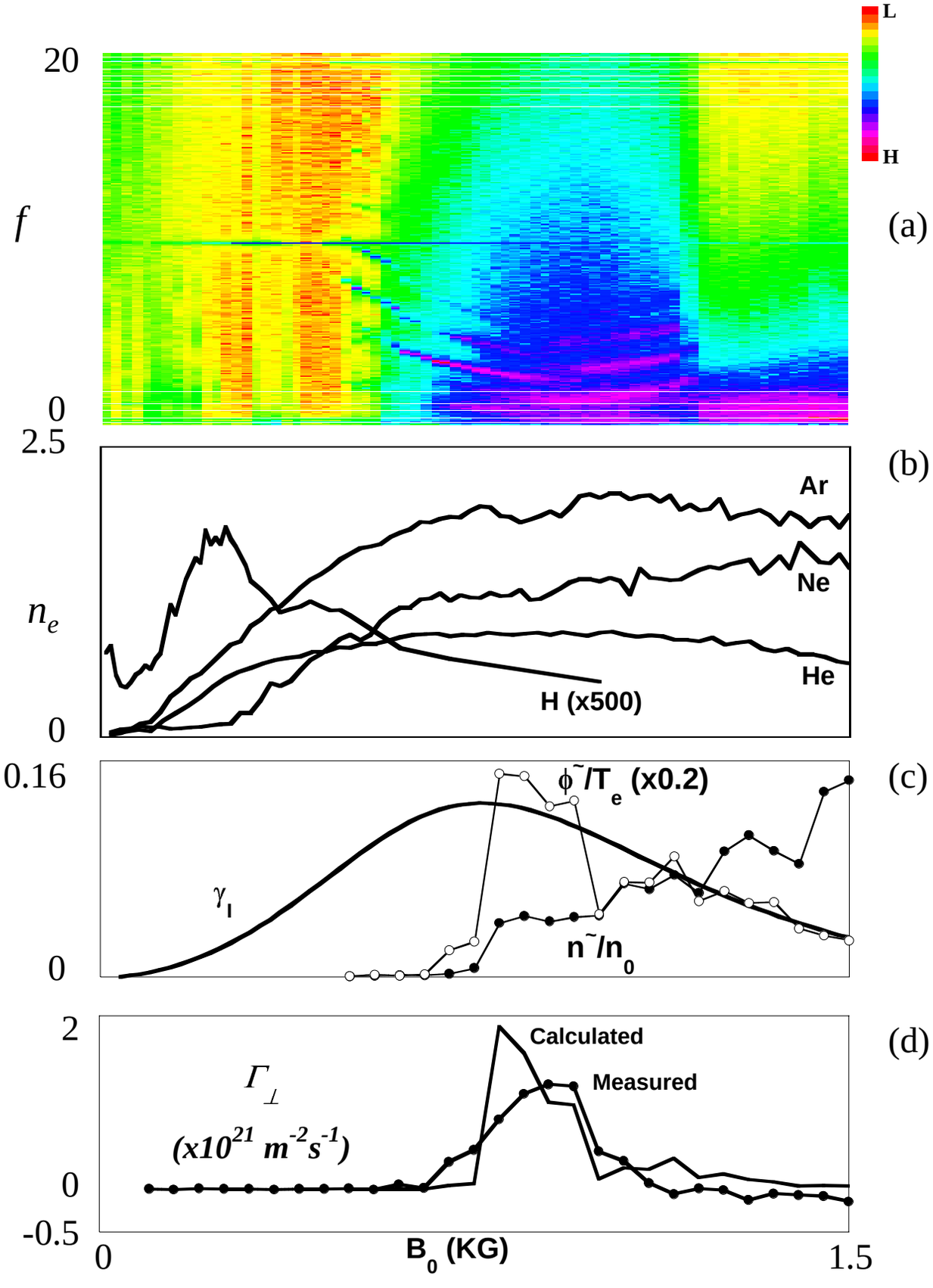
L
H
20
f
0
(a)
2.5
n_e
0
Ar
Ne
He
H (x500)
(b)
0.16
0
γ_I
$\tilde{\phi}/T_e$ (x0.2)
$\tilde{n}/n_0$
(c)
2
0
-0.5
$\Gamma_\perp$
$(x10^{21}\ m^{-2}s^{-1})$
Calculated
Measured
(d)
0
B_0 (KG)
1.5

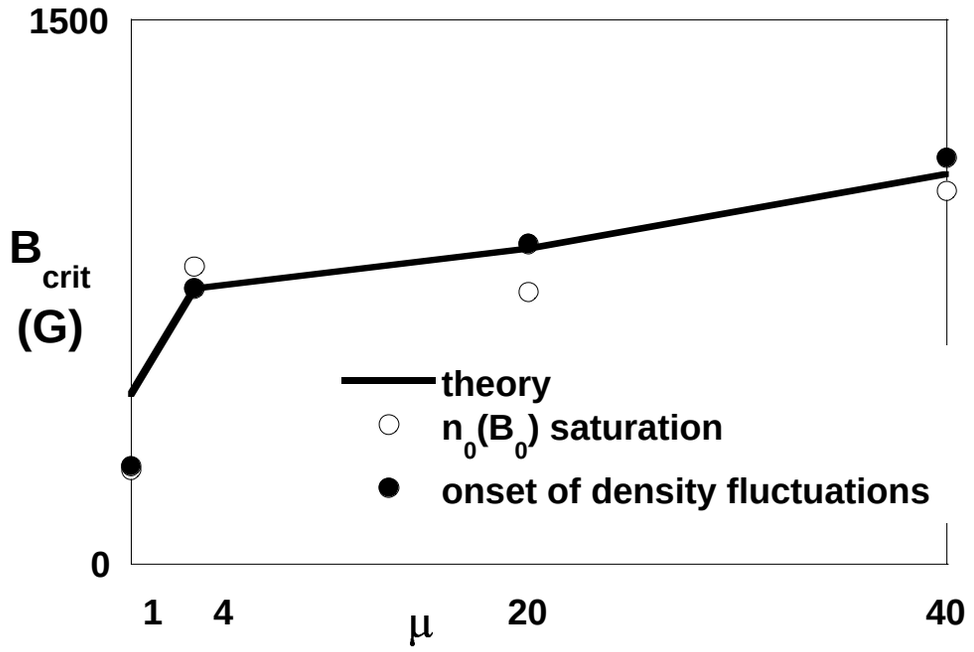
1500
B
crit
(G)
0
1
4
μ
20
40
theory
n0(B0) saturation
onset of density fluctuations

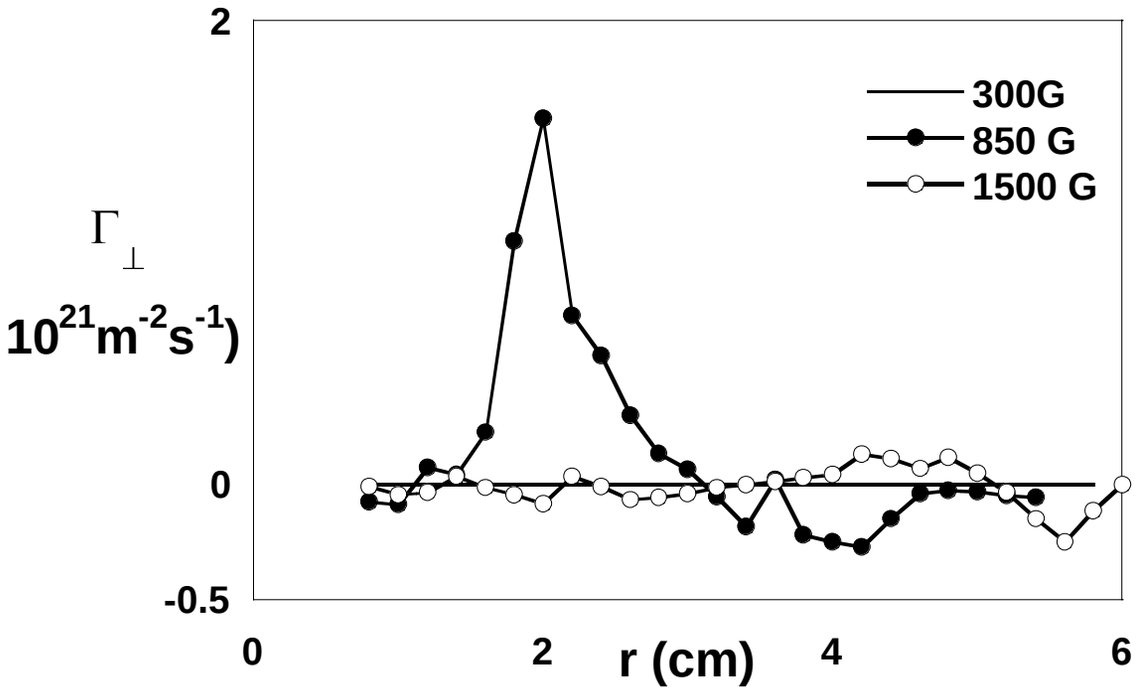
2
0
-0.5
0
2
4
6
r (cm)
$\Gamma_\perp$
$10^{21}m^{-2}s^{-1}$)
300G
850 G
1500 G

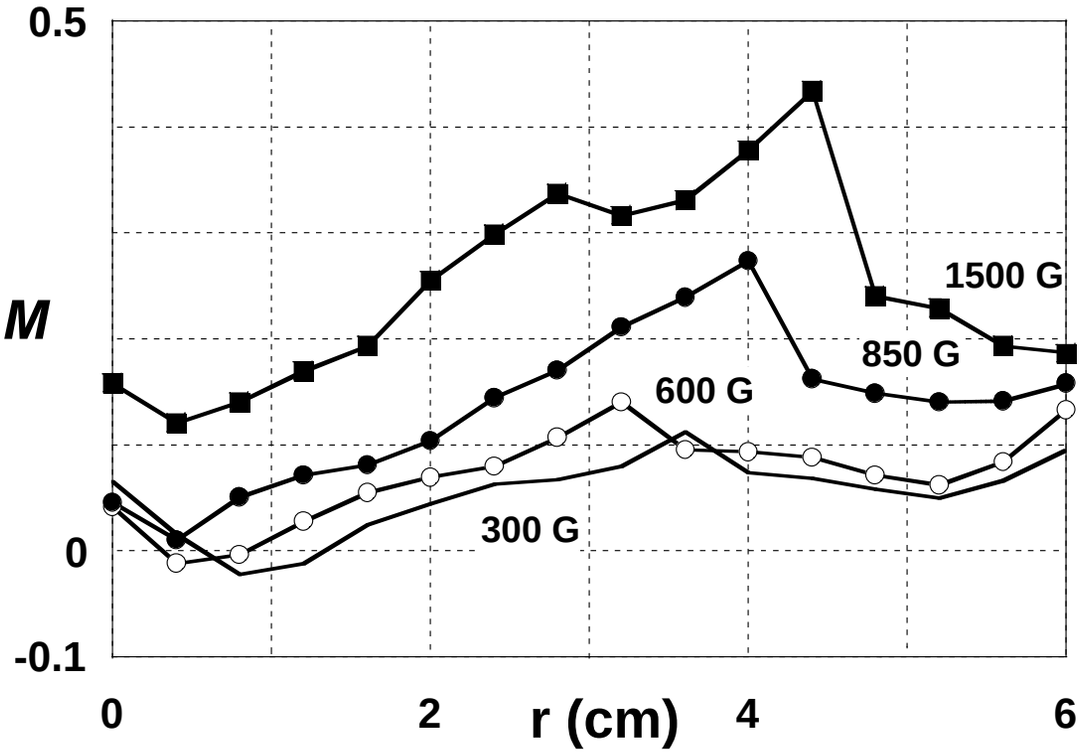
0.5
M
0
-0.1
0
2
r (cm)
4
6
1500 G
850 G
600 G
300 G